Macromolecules

Article

pubs.acs.org/Macromolecules

Spectroscopic Signature of Two Distinct H-Aggregate Species in Poly(3-hexylthiophene)

Fabian Panzer,[†,‡] Michael Sommer,[§] Heinz Bässler,[‡] Mukundan Thelakkat,[§] and Anna Köhler*[,†,‡]

[†]Experimental Physics II, [‡]Bayreuth Institute of Macromolecular Research (BIMF), and [§]Applied Functional Polymers, Macromolecular Chemistry I, University of Bayreuth, 95540 Bayreuth, Germany

Supporting Information

ABSTRACT: In an endeavor to correlate the optoelectronic properties of π-conjugated polymers with their structural properties, we investigated the aggregation of P3HT in THF solution within a temperature range from 300 to 5 K. By detailed steady-state, site-selective, and time-resolved fluorescence spectroscopy combined with Franck–Condon analyses, we show that below a certain transition temperature (265 K) aggregates are formed that prevail in different polymorphs. At 5 K, we can spectroscopically identify two H-type aggregates with planar polymer backbones yet different degree of order regarding their side chains. Upon heating, the H-character of the aggregates becomes gradually eroded, until just below the transition temperature the prevailing "aggregate" structure is that of still phase-separated, yet disordered main and side chains. These conclusions are derived by analyzing the vibrational structure of the spectra and from comparing the solution spectra with those obtained from thin films that were cooled slowly from the melting temperature to room temperature and that had been analyzed previously by various X-ray techniques. In addition, site selectively recorded fluorescence spectra show that there is—dependent on temperature—energy transfer from higher energy to lower energy aggregates. This suggests that they must form clusters with dimensions of the exciton diffusion length, i.e., several nanometers in diameter.

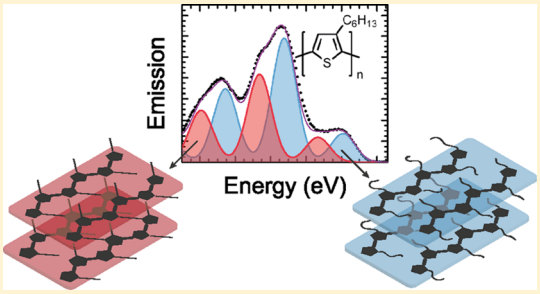

1. INTRODUCTION

A characteristic feature of organic solids is that electronic coupling among the constituting elements is weak yet it controls their optoelectronic properties. Deliberate or unintentional modification of the morphology has therefore a significant impact on the electronic properties such as the transport of charge carriers and the dissociation of excitations, i.e., excitons.[1−4] Currently there is strong endeavor toward understanding and controlling the relation between film morphology and electronic structure in devices such as solar cells and field effect transistors, using conjugated polymers as active elements, with a view to improve their performance.[5,6] Even though, understanding the formation of self-assembled structures in rigid or semirigid conjugated polymers which are typically processed out of solution is still less studied, especially compared to the large body of work established for flexible, nonconjugated polymers.

A material that emerged as a workhorse, notably in field of organic photovoltaics,[7−11] is regioregular poly(3-hexylthiophene) (P3HT). Since the discovery that in regioregular P3HT the charge carrier mobility measured in the field effect transistor configuration is much higher than in regiorandom P3HT,[12−14] much effort is currently spent on the understanding and improvement of structural order on P3HT. Depending on solvent, temperature, molecular weight, and sample preparation, it can exist in an amorphous phase with coiled chain conformations or in an aggregated phase containing planarized chains with some propensity to form semicrystalline domains.[11] These aggregates can be of an H-type or of a J-type nature, depending on the strength of interchain to intrachain coupling. The transition from one coupling regime to the other—reported in particular for P3HT nanofibers—depends sensitively to molecular weight and regioregularity of the sample.[15−18] It is also well established that P3HT can adopt different morphologies; i.e., it is polymorph.[19−23] In different morphologies, the separation and orientation of the polymer segments are different with the consequence that the electronic properties depend on the morphology.[24]

It is important to realize that, while being a workhorse, P3HT is not a singular case but rather a model for other technologically useful conjugated polymers. All of them have more or less stiff backbones and are therefore prone to adopt semicrystalline morphologies. For example, the poly(*p*-phenylene) derivative MEH-PPV has been shown to undergo a similar disorder–order phase transition upon cooling a solution similar P3HT,[25] and the polyfluorene derivative PFO is well-known for adopting an amorphous phase or an ordered β-phase.[26]

In structural studies including various techniques of X-ray diffraction and microscopy, different polymorphs of P3HT-

Received: January 21, 2015
Revised: February 18, 2015
Published: February 27, 2015

DOI: 10.1021/acs.macromol.5b00129
Macromolecules 2015, 48, 1543−1553

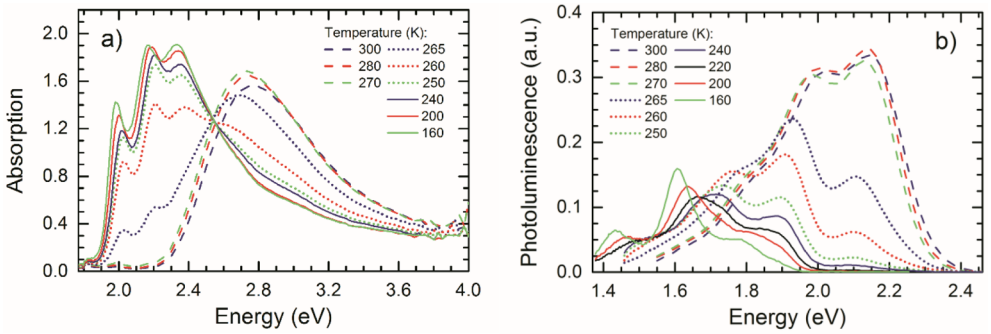

Figure 1. Absorption (a) as well as fluorescence spectra (b) of P3HT in THF solution for different temperatures. Spectra that belong to the three inherent temperature ranges described in the text are indicated with different lines (dashed, dotted, and straight). Emission spectra were corrected for the relative changes in absorption at 3.06 eV (being the excitation energy for all fluorescence spectra).

aggregates have been identified. For example, the work of Prosa et al. and Mena-Osteritz et al. identified H-aggregates with interdigitated side chains that form on graphite surfaces or, to a small amount, under certain spin-casting conditions.[27,28] They can also be prepared by self-seeding approaches.[29] This polymorph of P3HT is frequently referred to as "form II".[23,27] More common, however, are H-aggregates with noninterdigitating, noncrystalline side chains,[27,30−32] also known as "form I".[23,27] They form in a layer structure of separated main and side chains, where the main chains may adopt either a liquid, smectic-like packing, or a regular, crystalline packing. While the latter is thermodynamically more stable, its formation is frequently kinetically hindered.

These structural techniques provide valuable insight into the existing polymer morphologies and their formation processes. They can, however, be too elaborate or time-consuming to be applied routinely to the characterization of films that are to be used in device structures. A comparatively fast and simple approach to identify the presence of different H-aggregates in films (or solutions) is to measure their fluorescence spectra, yet this method requires that the spectral signatures of different polymorphs be known.

Here, we have studied the formation of H-aggregates in solution of tetrahydrofuran (THF) upon continuous cooling from room temperature to 5 K with the aim to identify the evolution of their spectral signatures. We find that the spectral shape of the H-aggregate emission evolves continuously. From the first appearance of aggregate emission at 265 K, the spectrum changes from a vibrational structure that essentially matches that of a nonaggregated chain to one with a strongly suppressed 0−0 transition peak at 160 K and below. Importantly, closer inspection identifies emission from two distinct, coexisting polymorphs. Notably, these two polymorphs are not the "form I" and "form II" mentioned in the literature (ref 19). Rather, they are two variants of "form I". Thus, the fluorescence features are assigned to H-aggregates in a layer structure of separated main and side chains. In both polymorphs, the main chain is crystalline and the side chains are noninterdigitated. Higher energy emission results for a polymorph with disordered side chains while lower energy emission is observed for a polymorph with crystalline (and still noninterdigitated) side chains. Emission from both polymorphs is also observed and assigned to in neat thin films, which is the form in which P3HT is used in optoelectronic devices.

2. EXPERIMENTAL SECTION

2.1. Sample Preparation. For our studies, we used P3HT synthesized by a modified Grignard metathesis reaction method as described elsewhere.[33] Because of this synthetic method, the sample has a very narrow molar mass distribution and thus a very low dispersity index (D = 1.16). The number-average molecular weight (M_n = 18 600 g/mL) and the weight-average molecular weight (M_w = 21 600 g/mL) were measured by gel permeations chromatography (GPC) in tetrahydrofuran (THF) with polystyrene as a calibration standard. The number of repeating units was determined to 74 ± 2 by MALDI-TOF measurements. The sample thus contains exactly one tail-to-tail defect that is distributed along the entire chain.[34] For all solution measurements, we dissolved the polymer in THF at a concentration of 0.2 mg/mL. To ensure that all of the polymer chains are completely dissolved, the solution was heated to 40−50 °C and stirred for about 30 min, so that no macroscopic particles could be observed any more. For the measurements, the solution was filled in a 1 mm cuvette that could be sealed and inserted into a cryostat.

To carry out measurements on thin films, two films of P3HT were spin-coated with 2000 rpm for 60 s from 10 mg/mL THF solution onto silicon wafers covered with a natural oxide layer in nitrogen atmosphere. One film was heated subsequently in nitrogen atmosphere to 250 °C, i.e., above the melting temperature of P3HT at 230 °C,[30] and cooled slowly to room temperature at a rate of 1 K/min using a programmable heating plate (Model HP60 from Torrey Pines Scientific Inc.). In contrast to that, the other film was used without any further treatments after spin-coating.

2.2. Steady-State Absorption and Emission Measurements. To measure steady-state absorption as well as emission spectra for different temperatures, we used a home-built setup that allows us to record absorption and fluorescence spectra at the same sample spot immediately after each other for each temperature step. In brief, the sample (a 1 mm cuvette with solution or a film) was placed in an Oxford Instruments cryostat. Sample heating or cooling was done in a stepwise fashion with a rate of about 2 K/min and an equilibration time of 30 min before taking the measurement. For absorption measurements, the light from a xenon lamp was dispersed through a first monochromator M1, transmitted through the sample, dispersed through a second monochromator M2, and eventually recorded by a silicium diode connected to a lock-in amplifier.

For emission measurements a flip mirror switched the incident light to a diode laser with excitation wavelength 405 nm. The laser beam was incident onto the sample at an angle of about 60° to the normal. The resulting fluorescence was dispersed through the monochromator M2 and recorded by the silicium diode connected to the lock-in amplifier. The spectra were corrected for the transmission of the setup. A more detailed description of the setup can be found elsewhere.[35]

To measure the emission in a site selective fashion, we replaced the diode laser by a pulsed Nd:YAG laser with a pulse width of 7 ns. Tunable excitation was obtained by converting the 355 nm pulse by an optical parametric oscillator from GWU that covers a continuous spectral range from 410 to 710 nm. The resulting emission was then

DOI: 10.1021/acs.macromol.5b00129
Macromolecules 2015, 48, 1543−1553

recorded using a glass fiber connected to a spectrograph (Oriel MS125) with an attached CCD camera (Andor iDus DU420).

2.3. Time-Resolved Emission Measurements. Time-dependent emission spectra were recorded using a streak camera setup, with the sample held again in a cryostat from Oxford Instruments. Light from a 80 MHz pulsed Chameleon II laser from Coherent was frequency doubled by a second-harmonics generator to provide an excitation energy of 3 eV. The emitted light was diffracted through an Acton SP-2300i spectrograph and eventually recorded by an Optronis SC-10 streak camera combined with a TSU12-10 deflection unit and a SRU-BA detection unit.

3. RESULTS

3.1. Temperature Dependence of the Aggregate Emission. For a detailed spectroscopic investigation of the P3HT electronic structure in the aggregated phase, we measured absorption as well as emission spectra in THF solution within the temperature range from 300 K down to the melting point of THF (Figure 1), which is at about 160 K.[36] As discussed in detail in previous work,[35] P3HT undergoes a disorder−order transition upon cooling. In the spectra shown in Figure 1, three regimes can be discerned. In the temperature range from 300 to 270 K, i.e., above the phase transition temperature, the absorption spectra are broad and structureless, indicating that the chains are disordered.[14,37] The bathochromic shift by 40 meV of the maxima and the increase in intensity of about 7% that is observed upon cooling from 300 to 270 K indicate an increased conjugation length that suggests a swelling-up process of the chain backbone. This red-shift and intensity increase are also reflected in the associated fluorescence spectra, which are overall more structured, featuring a $S_1 \rightarrow S_0$ 0−0 emission peak at 2.15 eV and a vibrational satellite at about 2.0 eV. When lowering the temperature from 265 to 250 K, a vibrationally resolved absorption spectrum appears with a $S_1 \leftarrow S_0$ 0−0 feature at 2.0 eV. The spectra at different temperatures feature an isosbestic point at 2.53 eV. This is the signature of the occurrence of a phase transition from the disordered to a more ordered phase.[35] The associated changes in the fluorescence spectra have been attributed to the emergence of an additional emission feature with a 0−0 peak at 1.90 eV that overlaps with the 0−1 emission feature of the disordered phase and that grows in relative intensity at the expense of the emission from the disordered phase upon cooling to 250 K. This additional emission has been assigned to the fluorescence of the ordered phase. Upon subsequent cooling in the temperature range below the phase transition, i.e., from 240 to 160 K, the 0−0 absorption peak of the ordered phase shifts toward lower energies and becomes more intense, while the 0−0 emission peak of the ordered phase appears to reduce in intensity. Both absorption and emission spectra feature a very similar bathocromic shift.

The analysis and interpretation of the development evident in the spectral part attributed to the aggregated phase require a deconvolution of the emission from disordered and ordered phases. The procedure is illustrated in Figure 2. We consider that the fluorescence spectrum well above the phase transition temperature, e.g. at 280 K, contains only emission from the disordered phase. To confirm this, Figure 2a illustrates that the 280 K fluorescence spectrum can be modeled satisfactorily in terms of a Franck−Condon progression.[38] This implies that the energy dependence of the photoluminescence $P(\hbar\omega)$, normalized to the cube of the refractive index n (assumed to be constant within the investigated spectral range), to the cube

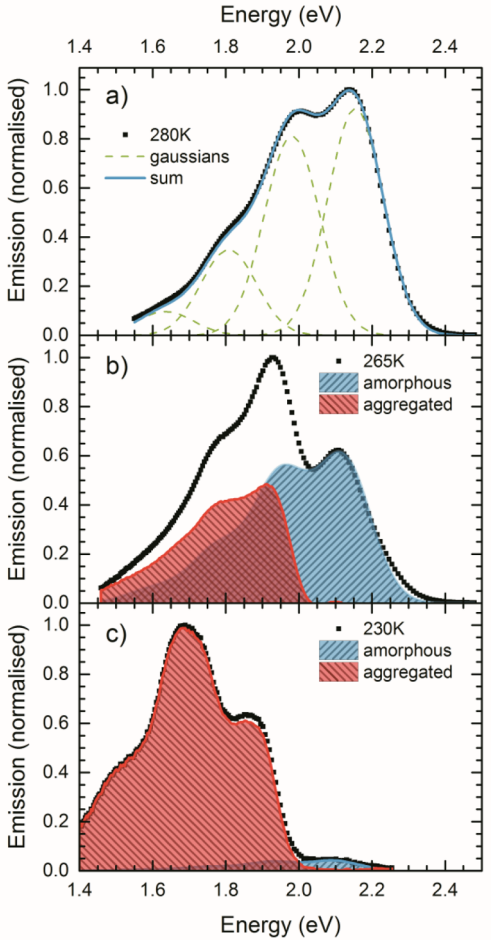

Figure 2. Illustration of isolating the fluorescence spectra of the aggregate phase at selected temperatures. (a) The 280 K fluorescence of the amorphous phase (black squares) is modeled by a Franck−Condon analysis (blue solid line) using an effective mode (green dashed line). (b, c) The 280 K spectrum (blue) is scaled to the high-energy tail of the 265 and 230 K emission spectra (black squares). The difference between the two spectra (red) is assigned to emission from the aggregated phase.

of the photon energy $\hbar\omega$ and to the intensity of the 0−0 vibrational peak I_{0-0}, is given by

$$\frac{P(\hbar\omega)}{n^3(\hbar\omega)^3 I_{0-0}} \sim \sum_{m=0} \frac{S^m}{m!}\Gamma\delta[\hbar\omega - (E_0 - mE_d)] \quad (1)$$

where $S = 1.1$ is the Huang−Rhys factor of an effective vibrational mode with energy $E_d = 0.175$ eV,[4] Γ is the Gaussian line width function with the standard deviation σ, and E_0 denotes the energy of the 0−0 transition. Once the phase transition sets in, i.e., for temperatures below 265 K, the spectra cannot be modeled as progressions from one emitting state. As mentioned above, we consider the spectra to result from the superposition of emission from the disordered and ordered, aggregated phase. To isolate the emission from the aggregated phase, the 280 K emission spectrum is scaled to the high-energy side of the actual emission spectra between 265 and 160 K (here changes in E_0 and σ were allowed to account for the temperature dependency of these two parameters; see Figure S1 in the Supporting Information) and subtracted. The remaining emission is attributed to the aggregate phase (Figure 2b,c).

DOI: 10.1021/acs.macromol.5b00129
Macromolecules 2015, 48, 1543−1553

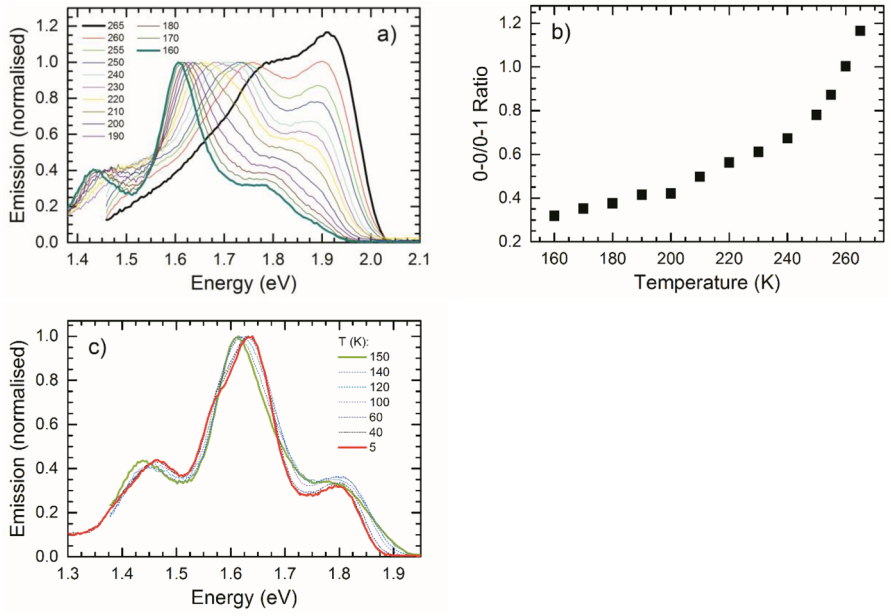

Figure 3. (a) Fluorescence spectra of aggregated P3HT in the temperature range from 265 to 160 K where the polymer chains are in fluid solution. The spectra are normalized to the intensity of the $S_1 \rightarrow S_0$ 0−1 feature. (b) Temperature dependence of the ratio of the 0−0/0−1 features of the $S_1 \rightarrow S_0$ transition in the same range. (c) Fluorescence spectra of aggregated P3HT recorded at temperatures between 160 and 5 K, where THF is crystalline.

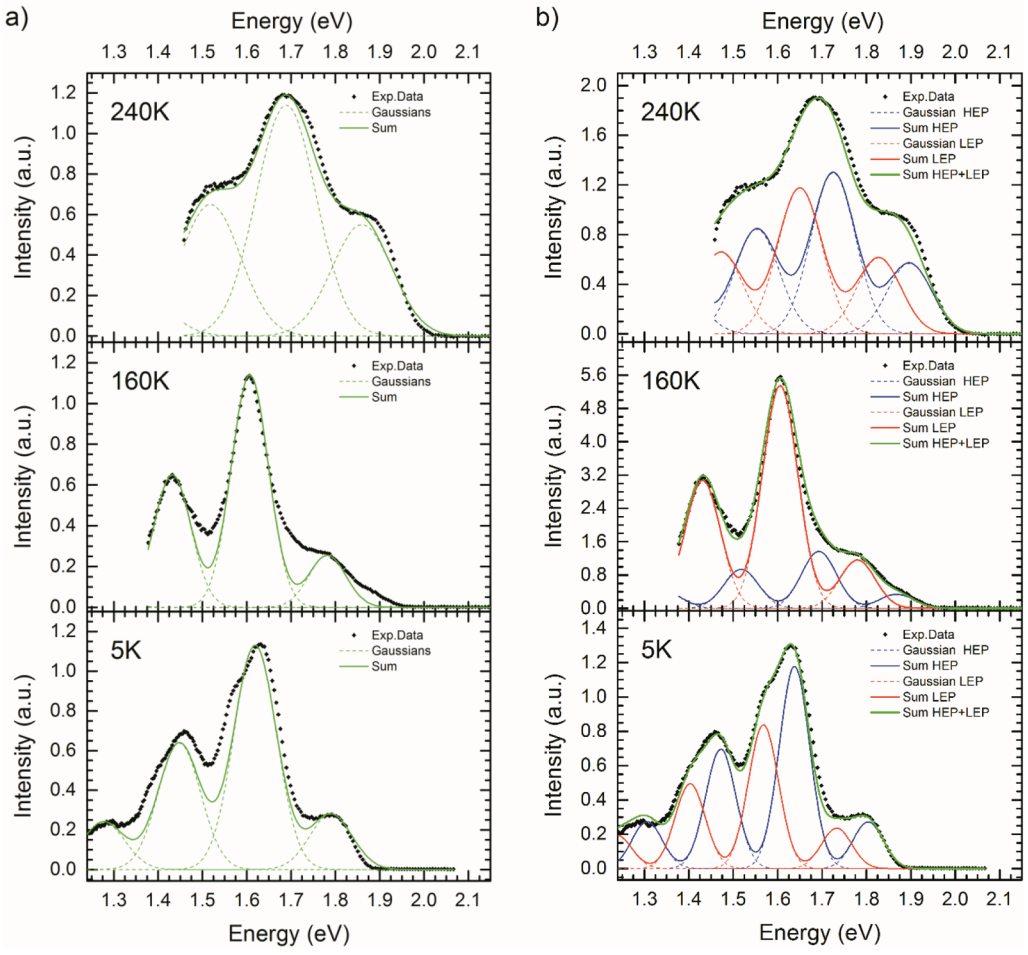

Figure 4. (a) Modified Franck−Condon analysis according to eq 2 (green solid line) of the fluorescence spectra (black squares) of P3HT aggregates at 240, 160, and 5 K using a single vibronic progression (green dotted line). (b) The same as in (a) but using a superposition of a higher energy progression (HEP) (blue solid line) and a lower energy progression (LEP) (red solid line).

DOI: 10.1021/acs.macromol.5b00129
Macromolecules 2015, 48, 1543−1553

Figure 3a shows the normalized spectra of aggregate emission in the temperature range of 265−160 K. Note the change in abscissa scale between Figures 2 and 3. The spectra show a pronounced 0−0 feature at 1.9 eV, which shifts to 1.77 eV while decreasing the temperature down to 160 K. Remarkably, the ratio of the 0−0/0−1 vibrational peak intensities decreases continuously from about 1.2 at 265 K to 0.3 at 160 K (Figure 3b). Additional emission spectra were also measured for the temperature range between 160 and 5 K (Figure 3c). Since below 160 K THF is in a crystalline phase,[36] the spectra correspond to P3HT chains embedded in a rigid THF matrix. This preludes major conformal changes. Accordingly, there is only a minor bathochromic shift when decreasing the temperature from 150 to 5 K. In this temperature range it was not possible to measure absorption spectra because the THF matrix is opaque.

3.2. Evidence for Two Different Aggregate Phases. While the deconvolution of the fluorescence spectra described above is sufficient for an overall assessment of evolution of the character of the aggregates, it is unable to account for important details regarding the identification of their structure. For this reason we carried out a modified (compared to eq 1) Franck−Condon analysis based upon the approach by Clark et al.[39] It takes into account the decrease of the 0−0 peak intensity in the fluorescence spectra when the chromophores form H-aggregates. The fluorescence is then described by

$$\frac{P(\hbar\omega)}{n^3(\hbar\omega)^3} \sim \alpha\Gamma(\hbar\omega - E_0) + \sum_{m=1} \frac{S^m}{m!}\Gamma\delta \times [\hbar\omega - (E_0 - mE_d)] \quad (2)$$

The term $\alpha\Gamma(\hbar\omega - E_0)$, in which α is the scaling factor, accounts for the fact that in a disordered H-aggregate the 0−0 feature of the fluorescence spectrum is suppressed. For a perfectly ordered H-aggregate, α would be zero since the 0−0 transition was symmetry-forbidden. The symbols take the same meaning than for eq 1. The scaling factor α, the energy E_0 of the 0−0 transition, and the standard deviation σ of the Gaussian line width were allowed to change with temperature, while the Huang−Rhys parameter S = 1.1 and the effective vibrational mode energy E_d = 0.175 eV were kept constant. Figure 4a shows three emission spectra at representative temperatures. While the spectrum at 240 K can be described satisfactory by a single progression with one effective vibrational mode, deviations between the Franck−Condon analysis and the experimental data appear at 160 K. In particular, the data show an additional shoulder at 1.9 eV and a less structured spectral shape that cannot be accommodated when using one progression. Using additional and/or different vibrational modes does not help to overcome these deviations in spectral shape and furthermore cannot be used to explain the additional observed emission intensity in the range of 1.9 eV, being higher than the proposed 0−0 energy at 1.8 eV. At 5 K, the vibrational peaks at 1.62 and 1.45 eV carry additional low-energy shoulders that cannot be modeled in terms of a single Franck−Condon progression, even when hypothetically considering additional/altered vibrational modes.

As an alternative approach, we considered the superposition of two similar, modified Franck−Condon progressions according to eq 2, i.e., a higher energy progression (HEP) with a 0−0 transition centered at about 1.9 eV for the 160 K spectrum and a lower energy progression (LEP) shifted by about 80 meV to lower energies (see Figure 4b). It turns out that the superposition of the HEP and LEP provides an excellent fit to the experimental spectra in the entire temperature range, while analyzing the low-temperature spectra in terms of a single modified Franck−Condon progression was unsuccessful. Figure 5 shows the relevant spectral parameters.

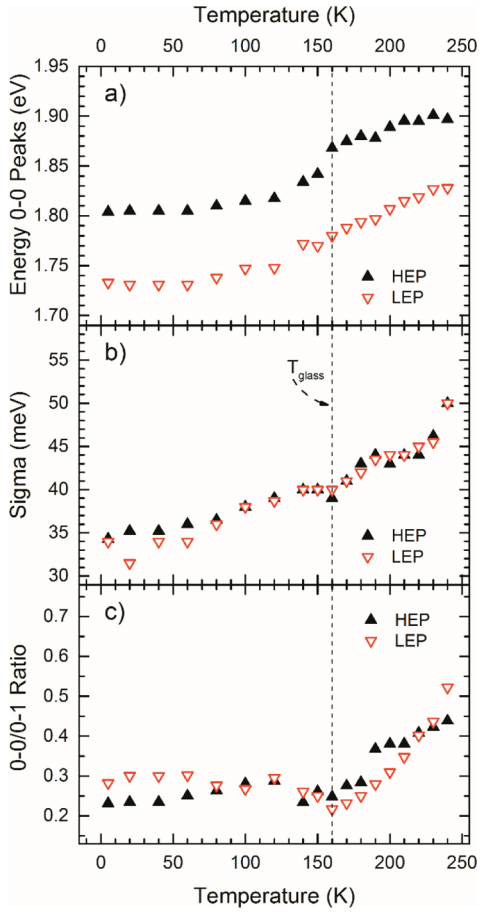

Figure 5. Fit parameters derived from the modified Franck−Condon analysis of the fluorescence spectra of P3HT aggregates using two energetic different progressions (HEP, LEP) as a function of temperature. (a) Energies of the 0−0 emission, (b) standard deviations σ of the 0−0 feature, and (c) ratio of 0−0 and 0−1 emission. The dashed vertical line indicates the glass transition temperature of THF.

The 0−0 energy of the LEP (HEP) fluorescence spectrum shifts from 1.91 eV (1.83 eV) at 240 K to 1.8 eV (1.72 eV) to 5 K, while the energy difference between the HEP and the LEP is temperature independent (Figure 5a). Within the experimental uncertainty both the Gaussian disorder parameter σ and the ratio of 0−0/0−1 emission peaks are the same for the HEP and LEP. The disorder parameter decreases continuously from 50 meV at 240 K to 35 meV at 5 K (Figure 5b). The 0−0/0−1 ratios behave similarly and decrease as a function of temperature, starting at values at around 0.5 at 240 K and saturating in the range of 0.23−0.28 for the lowest temperatures (Figure 5c). Thus, the spectral analysis of the fluorescence spectra suggests the spectra to arise from the superposition of two emissions that have the same H-type nature and that are subject to the same inhomogeneous broadening yet that differ in transition energy by about 80 meV.

The necessity to involve two Franck−Condon progressions instead of only one is also borne out by an analysis of the absorption spectra. To do this, we use a modified Franck−

DOI: 10.1021/acs.macromol.5b00129
Macromolecules 2015, 48, 1543−1553

Condon Fit developed by Spano et al.[40−43] which takes into account the influence of intermolecular coupling on the absorption spectrum of aggregates.

$$\frac{A(\hbar\omega)}{n(\hbar\omega)} \sim \sum_{m=0} \frac{S^m}{m!}\left(1 - \frac{We^{-S}}{2E_d}\left(\sum_{n\neq m} \frac{s^n}{n!(n-m)}\right)\right)^2 \times \Gamma\delta[\hbar\omega - (E_0 + mE_d)] \quad (3)$$

where W defines the exciton bandwidth (and n being the vibrational quantum number).

The difference between the Franck−Condon (FC) progression simulating the absorption of the aggregated phase and the experimental spectra, i.e., the residue, should represent the absorption spectrum of P3HT in the disordered phase. We find that similar to the case of emission, modeling the spectra using only one progression (see Figure S2 in the Supporting Information) is unsuccessful. The sharp 0−0 peak at about 1.9 eV limits the Gaussian line width of the Franck−Condon analysis and results in a residue that reveals a vibronic progression and overall shape that are at variance with the absorption spectra of the disordered phase shown in Figure 1a. Successful modeling of the absorption spectra is, however, possible by using a superposition of two progressions according to eq 3. The two progressions have a spectral offset of about 100 meV, comparable to that in emission. Figure 6 shows the absorption measured at 160 K, along with the two FC progressions, their superposition, and the residue. The progressions used an exciton bandwidth of W = 70 meV. Analogous to the simulation of the fluorescence spectra of the aggregates, we used constant values of S = 1.1 and E_d = 0.175 eV while the energy E_0 of the 0−0 transition and the standard deviation σ of the Gaussian line width were allowed to change with temperature. Using two progressions, the residue matches well with the absorption of disordered P3HT (cf. Figure 1a). Thus, the analysis of the absorption spectra corroborates the conclusion of two H-aggregates drawn from the analysis of the fluorescence spectra.

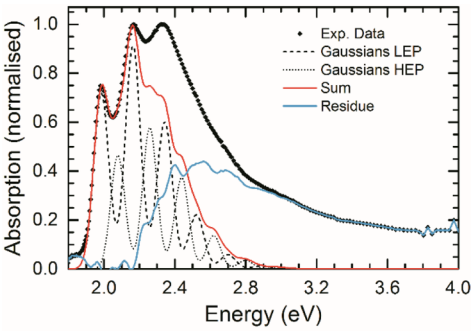

Figure 6. Absorption spectra of P3HT (black squares) at 160 K as well as the Franck−Condon analysis (red solid line) according to eq 3 using two progressions (black dashed and dotted lines).

The temperature dependence of the Gaussian disorder parameter σ as well as the energy E_0 of the $S_1 \leftarrow S_0$ 0−0 transition obtained from the analyses of the absorption and emission spectra are compared in Figure 7 for the lower energy progression LEP. The data for the higher energy progression HEP are analogous. Both parameters, σ as well as E_0, continuously decrease while cooling down the solution, with E_0 decreasing by 60 meV from 2.04 eV at 260 K down to 1.98 eV for 160 K (Figure 7a), and σ reducing by 14 meV from 57 meV toward 43 meV within the same temperature range (Figure 7b). The Stokes shift between the 0−0 features in absorption and emission is about 200 meV almost independent of the temperature (see Figure S3 in the Supporting Information). This comparable evolution of the progressions in absorption and emission is consistent with the existence of two H-aggregates that differ only slightly.

Further evidence for the presence of two different aggregate phases is derived from experiments employing the site selection technique. When scanning the excitation energy E_{ex} from 2.070 to 1.865 eV, the fluorescence spectra change in a characteristic way (Figure 8). This is most obvious in the 5 K emission spectrum. For excitation within a spectral range from 2.070 to 1.938 eV, the fluorescence spectrum changes only marginally and is characteristic of the higher energy (HEP) aggregate. When exciting at 1.908 eV a low-energy shoulder on the 0−1 feature appears. Upon further decreasing of E_{ex} to 1.865 eV, the 0−1 feature of HEP shifts by approximately 20 meV because tail states of the distribution of HEP states are addressed. In addition to this, the 0−1 transition of the lower energy aggregate (LEP) spectrum becomes the dominant feature. This is an unequivocal proof that the HEP and LEP emissions originate from different aggregates. It also demonstrates that at 5 K there is little communication between the two different aggregates. Otherwise, the fluorescence from the lower energy aggregates should be sensitized by exciting higher energy aggregates, contrary to experiment.

At 160 K, there are subtle differences in the evolution of the spectra upon scanning E_{ex} compared to the 5 K spectra. Again, the site selectively excited fluorescence from the aggregates is a superposition of emission from the higher energy progression

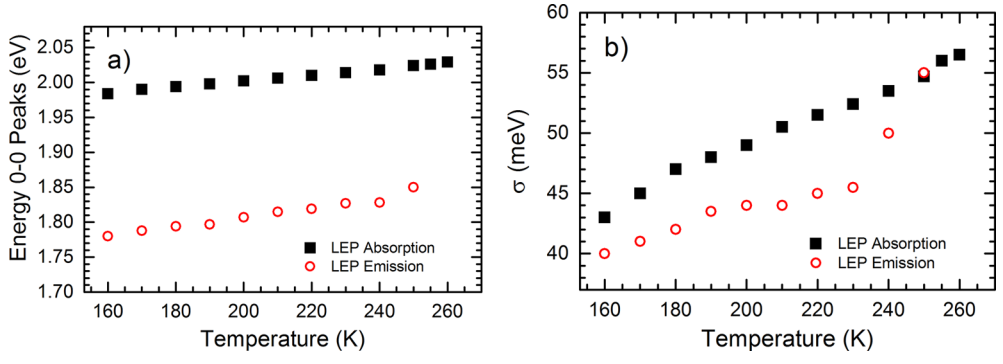

Figure 7. (a) Energies of the $S_1 \rightarrow S_0$ 0−0 peaks and (b) standard deviation σ for the low-energy progression (LEP) in absorption and emission.

DOI: 10.1021/acs.macromol.5b00129
Macromolecules 2015, 48, 1543−1553

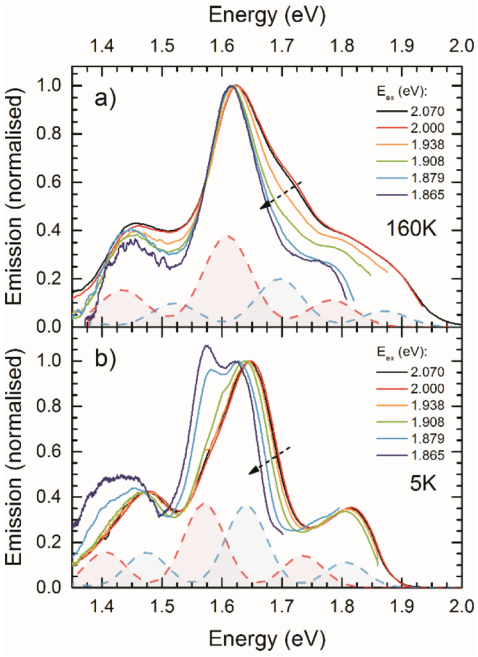

Figure 8. Fluorescence spectra (solid lines) of P3HT aggregates in THF parametric in the excitation energy E_{ex} (a) at 160 K and (b) at 5 K. The spectra are normalized to the intensity of the 0−1 feature. Spectra of corresponding HEP and LEP at those temperatures are also illustrated by dashed lines with filled area. The arrows indicate the direction of decreasing excitation energy.

and from the lower energy progression. In contrast to the 5 K spectra, the LEP is the dominant feature. Moreover, the spectral position of the LEP—traced most easily by considering its 0−1 peak at about 1.62 eV—remains nearly stationary when scanning E_{ex} from 2.070 to 1.865 eV, whereas the emission from the HEP shifts bathochromic by 18 meV (see Figure S4 for FC analysis on the site selected spectra). It seems that at 160 K there is temperature-dependent energy transfer from HEP to LEP which is frozen out at 5 K. This energy transfer from HEP to LEP at 160 K can also be seen when considering the time-dependent aggregate fluorescence spectra. Figure 9 shows spectra recorded within a time window of 15 ps for different times up to 6 ns after the excitation pulse at a temperature of 160 K. The spectra are normalized to unity at the approximate energy of the LEP 0−0 feature near 1.78 eV. It is evident how with increasing time the spectra reduce in

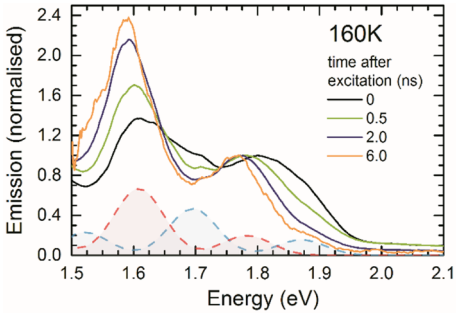

Figure 9. Normalized emission spectra (solid lines) of P3HT in THF for different times after the excitation pulse at 160 K. The spectra are normalized to unity at about 1.8 eV. For clarity, corresponding HEP and LEP are also illustrated by dashed blue and red lines.

relative intensity at the spectral positions corresponding to the 0−0 and 0−1 vibrational peaks of the HEP, i.e., at about 1.9 and 1.7 eV, whereas the relative intensity of the LEP 0−1 peak at about 1.6 eV increases. While a detailed analysis of the time dependence of this energy transfer is beyond the scope of the present paper, Figure 9 clearly corroborates the evidence for two emitting species brought forward by the site selectively recorded steady-state fluorescence spectra of Figure 8.

3.3. Nature of the Two Aggregate Phases. Having ascertained the occurrence of two distinct, albeit similar, H-aggregate phases for P3HT in THF at temperatures below the phase transition, we were wondering first whether it would be possible to assign the spectra to specific P3HT morphologies and second whether the two different aggregate phases of P3HT that we identified in solution can exist also in a bulk film. To answer this question, we recorded emission spectra of differently prepared P3HT films on silicon wafers at a temperature of 5 K for different excitation energies E_{ex}. One film ("heated") was heated to 250 C under nitrogen and then cooled down slowly as described in the Experimental Section, while the other one ("as cast") was measured as spin-coated without any further treatment (Figure 10). This sample preparation protocol follows the approach taken by Wu et al.,[30] who studied the morphology of such films by X-ray scattering.

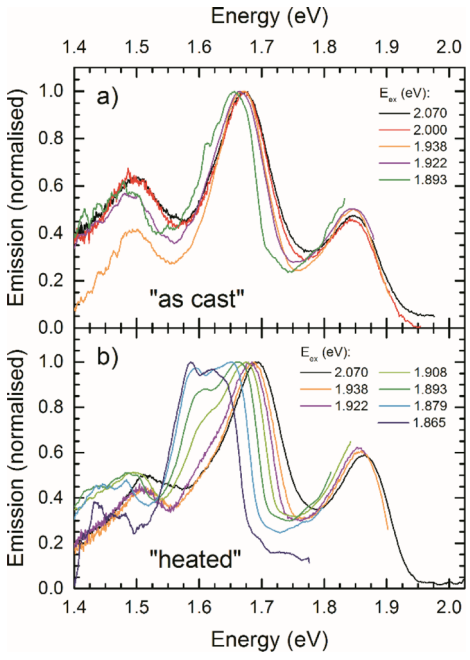

Figure 10. Normalized emission spectra of P3HT films at a temperature of 5 K for different excitation energies E_{ex}: (a) as-cast film; (b) a treated ("heated") film as described in the text.

The spectral shape of the emission spectrum of the "as-cast" film undergoes only minor changes when decreasing excitation energy E_{ex}. For excitation at 2.070 eV, it features a 0−0 vibrational peak at about 1.85 eV, a 0−1 peak at about 1.675 eV, and a 0−2 peak at about 1.50 eV. As evident most clearly when considering the 0−1 peak, the spectra shift to the red by only about 20 meV upon reducing the excitation energy by 177 meV to 1.893 eV. In contrast to this, the shape of the emission spectrum for the film, which was heated above its melting temperature, changes significantly for different excitation

DOI: 10.1021/acs.macromol.5b00129
Macromolecules 2015, 48, 1543−1553

energies. It appears to be made up by the superposition of two progressions. The higher energy progression has a 0−0 peak at about 1.85 eV and it is dominant for excitation at 2.070 eV, while roughly 80 meV below, a lower energy progression can be made out that is dominant for excitation at 1.865 eV. Analogous to the qualitative spectral changes for P3HT in THF at 5 K (Figure 8b), this LEP is first evident as an emerging shoulder in the 0−1 peak for excitation at 1.908 eV and then shifts to the red and becomes more and more intense for decreasing excitation energy. By comparing Figures 10b and 8b, it becomes obvious that the two aggregate phases (HEP and LEP) are formed both in THF solution and also when slowly cooling a P3HT film from above its melting temperature to room temperature.

4. DISCUSSION

The results obtained so far may be briefly summarized as follows. Figures 1−3 show that upon reducing the temperature of a THF solution of P3HT a transition from a phase with disordered chain conformations to a phase with ordered chains takes place. The emission from the ordered phase can be extracted, and it displays a continuous red-shift and concomitant reduction of the relative 0−0 peak intensity. From the analysis of the spectra in Figures 4−7, it becomes evident that absorption and emission of the ordered phase originate from two distinct, albeit similar, species. The two excitation features are both of the same H-type character (indicated by the same low value of the 0−0 peak intensity), are subject to the same degree of disorder (manifested in σ), and are separated by about 80 meV. The site-selective and time-dependent spectra of Figures 8−10 corroborate the evidence for two distinct excited states, which indicate that at elevated temperature energy transfer from the higher to the lower energy state can occur and that both H-type aggregates can also prevail in thin films when the processing conditions are chosen suitably.

4.1. Temperature Dependence of the Aggregate Emission. The emission spectra of aggregated conjugated polymers such as P3HT have been discussed in terms of the weakly interacting H/J aggregate model developed by Spano and co-workers.[39,42,44,45] This model considers chromophores that interact weakly by dipole−dipole coupling with a coupling energy that is less than the mean vibrational energy of the emission or absorption spectra. The resulting absorption and emission spectra of the H-type (= parallel dipole moments between the interacting chromophores) or J-type (= collinear dipole moments) aggregates still display a vibrational structure, albeit the intensities of the vibrational peaks are modified. In particular, the ratio between the 0−0 and 0−1 vibrational peaks depends strongly on the strength and character of the interchromophore coupling, yet also on the disorder present in the sample and on the sample temperature. In general, a 0−0/0−1 emission peak ratio that is enhanced compared to that prevailing in the nonaggregated chromophore indicates a J-type coupling, while a reduced emission peak ratio results from an H-type coupling. Upon reducing the temperature, the relative intensity of the 0−0 decreases (increases) further for a H-type (J-type) aggregate. The presence of disorder, quantified by the standard deviation σ of the inhomogeneously broadened Gaussian line shape, significantly moderates these effects.[46] We interpret the data shown in Figure 3a,b in this framework of weakly interacting H/J-aggregates.

The low-temperature emission spectrum taken at 160 K has a characteristic H-type aggregate character. This is evident from its vibrational structure that features a low 0−0/0−1 peak ratio and from the fact that it cannot be modeled using one or two common Franck−Condon progressions as expressed in eq 1. Rather, it requires the use of two similar, modified Franck−Condon progressions with reduced 0−0 peak as given by eq 2. Upon *raising* the temperature up to 265 K, the intensity of the 0−0 increases. Several factors contribute to this change in vibrational structure. (i) For a given value of interchain coupling and disorder in an H-aggregate, the relative intensity of the 0−0 peak increases with temperature and can approach the 0−0/0−1 ratio in the unaggregated molecule.[46] (ii) In addition, Figure 5b shows that in our sample the disorder itself increases with temperature, which further enhances the increase in the relative 0−0 intensity. (iii) This is intensified by thermal expansion upon heating, which increases the interchain distance thus reducing the interchain coupling. (iv) The observed hypsochromic shift upon raising the temperature suggests a reduction in conjugation length, implying an increase in interchain coupling that would counteract to some extent the increase in 0−0 caused by points i to iii.[46] The combination of these factors results in the observed overall increase in relative 0−0 peak intensity with temperature. Paradoxically at 265 K, the aggregate spectrum closely resembles that of a non-aggregated chain, except for the spectral position, as can be seen from Figure 2b. Evidently, the symmetry reasons that cause the 0−0 peak to vanish for a perfect weakly interacting H-aggregate at 0 K are lifted by temperature and disorder.

4.2. Evidence for Two Different Aggregate Phases. Testimony to the coexistence of two similar yet distinct weakly interacting H-type aggregates in THF solution is given (i) by the need to invoke two modified Franck−Condon progressions to model the emission and absorption data (Figures 4 and 6), (ii) by the ability to excite the two different aggregates selectively (Figure 8), and (iii) by the time-dependent fluorescence spectra at 160 K (Figure 9), where the spectral features at the position of the higher energy progression decay faster than the ones corresponding to the lower energy progression. These observations allow no other interpretation. The same two H-type aggregates also form in a thin film when it has been heated and allowed to cool slowly, while only one H-type aggregate prevails in a spin-cast film (Figure 10). Comparison of the spectra obtained from both films for excitation at 2.070 eV identifies the emission in the spin-cast film as arising from the higher energy progression. Thus, in a thin film structure, both polymorphs can be formed, yet the formation of the lower energy polymorph is kinetically hindered and requires suitable processing conditions. While several polymorphs of P3HT H-aggregates have been identified in structural studies, e.g., on the basis of wide-angle X-ray scattering and scanning tunneling microscopy,[23,27,28,30,31,47] the signatures of different polymorphs in optical spectroscopy have, to our knowledge, not been reported.

4.3. Nature of the Two Aggregate Phases. P3HT is known to exist in different phases that have been identified by structural studies.[27,28,30,31,47−49] Wu et al. used DSC, small-angle and wide-angle X-ray scattering, and AFM to investigate the structure of a P3HT film prepared in the same way and using material from the same batch as we use in our work.[30] They investigate the structural changes of P3HT upon cooling from the melt. In the isotropic melt, both the main chain and side chains are uncorrelated. For ease of reference, we shall call

DOI: 10.1021/acs.macromol.5b00129
Macromolecules 2015, 48, 1543−1553

this *phase 1*. It corresponds to morphology of the disordered phase in solution. Upon cooling below the melting point, the P3HT chains aggregate to form a layer structure of spatially separated main and side chains.[49] Both main and side chains are still disordered and liquid-like. We refer to this as *phase 2*. It exists only within a small temperature range until about 20 °C below the melting point. Upon further cooling, the main chains condense into a regular two-dimensional array. The polythiophene backbone is planar and crystallized while the side chains are still disordered (*phase 3*). Finally, when cooling below 50 °C, the chains adopt a three-dimensional crystalline topology with both main chains and side chains packed in a regular, ordered fashion (*phase 4*). By employing scanning electron microscopy and wide-angle X-ray scattering on P3HT nanowires and P3HT nanotubes in porous templates, Martín et al. confirm this basic sequence of structural ordering.[47] Very recently, the existence of two phases with planar backbone, one with ordered and one with disordered side chains, has also been reported by Brambilla et al. on the basis of Raman measurements.[48]

The phases 1 to 4 described here correspond to Figures 5e to 4b in Martín et al.[47] Note that the formation of the thermodynamically more favorable crystalline phases 3 and 4 can be kinetically hindered.[30] Independent of the processing method (cooling from melt, cooling a solution, reducing solution quality), the self-assembly process applies to about half of the material, with the other half remaining amorphous.[4,30,35]

These phases 1−4 are all characterized by side chains that are not interdigitated. In addition, a phase with interdigitated side chains has been reported (referred to as form II crystals). As mentioned above, such a structure can be formed under certain circumstances, e.g., on a graphite surface due to interfacial interactions,[28,31] when the polymer is subjected to other constraints during processing,[27] or in highly ordered single crystals grown from solution.[29] Since the interdigitated structure is accompanied by an increased π-stacking distance, it is easily converted, e.g. by moderate heating, to a thermodynamically more favorable structure with denser backbone packing, where π-stacking is optimized by placing the side chains into a noninterdigitated structure, tilted away from the backbone.[27,31] In particular, cooling from the melt leads to noninterdigitated structures.[27,30]

A key result of the present investigation is the recognition that in a P3HT film that has been slowly cooled from above the melting point to room temperature, the same two different H-aggregate species are found as in THF solution below the disorder−order phase transition. This is documented by Figures 8 and 10 and provides a link between the spectroscopy of those aggregates and their microscopic structure revealed in the recent structural studies. It allows to assign the fluorescence spectra of the higher energy (HEP) and lower energy (LEP) H-aggregates formed upon cooling P3HT in solution (see Figures 8 and 10). We can rule out an assignment of the HEP or LEP emission to an interdigitated H-aggregate structure for two reasons. First, as already mentioned, the interdigitated structure does not form upon cooling from a melt.[27,30] Second, in the interdigitated structure, the π-stacking distance is increased.[27,31] This would imply a reduced H-type coupling and thus concomitant a higher 0−0/0−1 ratio for the HEP or the LEP emission, at variance with experiment. Based on our observation that HEP and LEP emission are characterized by the same ratio of the 0−0/0−1 emission peaks (Figure 5), it is straightforward to attribute the HEP and LEP emission to phases 3 and 4, respectively. These are the aggregates with crystallized main chains yet disordered side chains and those with crystalline main and side chains. The two associated polymorphs have very similar interchain coupling, differing only regarding the degree of side-chain order.

The energy difference of about 70 meV between HEP and LEP is somewhat surprising. Evidently it arises from the fact that correlation between the laminar stacks is lost in phase 3 where the side chains separating the layers are disordered and liquid-like, while it is preserved in the phase 4 due to the crystalline side chains. Thus, this shift seems to reflect the impact of interactions between different lamellar stacks on the excited states energies, while ratio of the 0−0/0−1 emission peaks is controlled mostly by the interaction within one stack.

The conclusion that in phases 3 and 4 the polymer backbone is crystalline requires some specifying comment. In a molecular crystal such as an anthracene crystal, the S_1-S_0 0−0 transitions in absorption and emission are resonant, i.e., there is no Stokes shift, and they are homogeneously broadened. In contrast, this is not the case for the absorption and fluorescence spectra of the HEP and LEP features. By comparing Figures 1 and 5, it is evident that the 0−0 features of the fluorescence are offset from those in absorption by 100−200 meV, and they bear out an inhomogeneous broadening with a standard deviation of about 40 meV. The temperature-dependent Stokes shift can in part be attributed to spectral diffusion.[50,51] This spectral diffusion and the inhomogeneous broadening are clear evidence for the presence of energetic disorder. Such disorder can arise from two causes, namely a variation in the polarization of the environment or a variation in the conjugation length of the chromophore. Since inhomogeneous line broadening and spectral diffusion (Figures 5b and 5a, respectively) are identical for both polymorphs, it follows that the different degree of order in the side chains cannot be the main source for the energetic disorder. Thus, we argue that the polythiophene chromophores constituting the lamellar stack of H-aggregates do not have identical conjugation length. Rather, there is some distribution in conjugation length, despite the overall lamellar arrangement. Another contribution to the Stokes shift arises from the exciton band structure of the H-aggregate. In a disordered H-aggregate, absorption takes place to the top of the exciton band while emission occurs from its bottom. That bandwidth separation is roughly given by We^{-S}, where W is the free exciton bandwidth and S is the Franck−Condon factor.[42] Using the experimentally obtained values of W = 70 meV and S = 1.1, we obtain a value of 23 meV for this contribution to the Stokes shift.

Finally, we discuss whether and how the phase 2 relates to our spectroscopic measurements. Phase 2 is the structure that Wu et al. and Martin et al. reported to consist of spatially separated main and side chains without lamellar crystals. This phase prevails in samples when cooling from the melt for a small temperature range below the melting point only.[30,35] In the context of Figures 2b and 3a we already mentioned that there is a small temperature range just below the onset of aggregation upon cooling, say at 265 and 260 K, where the emission from the aggregate phase is clearly red-shifted from that of the disordered phase, yet the vibrational structures of the two emissions are nearly identical. It implies that the interchain coupling is already sufficiently strong to reduce the excited state energy, yet the prevailing disorder erodes any signature of an H-aggregate in the 0−0 to 0−1 peak ratio. The spectroscopic signature of the emission just below the onset of

DOI: 10.1021/acs.macromol.5b00129
Macromolecules 2015, 48, 1543−1553

aggregation is fully consistent with the morphology suggested for phase 2. We thus associate phase 2 with the emission spectra of the aggregated domains shown in Figure 3c. Obviously, upon further cooling this evolves into the crystalline phases 3 and 4 with the associated typical H-aggregate spectra showing the suppressed 0−0 peak.

4.4. An Estimate of the Domain Size. Having identified the polymorphs causing the HEP and LEP, we now consider which additional information we can extract from the site-selective and time-dependent experiments (Figures 8−10) regarding the microstructure of the P3HT H-aggregates. At 5 K, emission from phase 4 is observed when it is directly excited, e.g., by using an excitation energy of 1.865 eV. In contrast, when the excitation addresses phase 3, e.g., by exciting at 2.000 eV, emission is only seen from that phase, yet not from phase 4. Evidently, at 5 K, there is no energy transfer from the lamellar structure with still disordered side chains to the lamellae with crystalline side chains. This applies to both the neat film (Figure 10) and the frozen THF solution (Figure 8). Energy transfer from phase 3 to phase 4 does, however, occur when the temperature is raised to 160 K. For excitation at 2.070 eV, the dominant part of the emission is due to the lower energy all-crystalline phase 4, yet with a minor contribution from the actually excited phase 3 with the noncrystalline side chains (Figure 8). The time-dependent fluorescence spectra (Figure 9) indicate that this transfer takes place on a time scale of a few nanoseconds. These observations allow for an estimate regarding the size and distribution of the polymorphs.

(i) The appearance of energy transfer implies that the two polymorphs must be sufficiently close. For the concentration used here, this entails that an aggregated ensemble in solution must contain both polymorphs.

(ii) The facts that the energy transfer takes place not on an ultrafast time scale but rather on the comparatively slow nanosecond range and that some emission from the higher energy phase remains to be seen in the steady-state spectrum for excitation at 2.000 and 2.070 eV suggest that each polymorph must have a size that exceeds twice the exciton diffusion range at that temperature.

A typical exciton diffusion length at room temperature is about 5−10 nm.[52] However, in an inhomogeneously broadened density of states distribution the exciton diffusion length decreases with decreasing temperature.[53] Here the characteristic parameter is the ratio between the standard deviation of the Gaussian density of states distribution (σ) and k_BT. When decreasing σ/k_BT from 2 (equivalent to T = 300 K and σ = 52 meV) to 4 (equivalent to about 150 K), the exciton diffusion length decreases by a factor of roughly 5, i.e., to a value of 1−2 nm.[53] Thus, the observed energy transfer implies a polymorph size with a diameter exceeding a few nanometers. The overall structural picture that emerges is that of an aggregated ensemble that contains both a layered crystalline polymorph with crystalline side chains and one with disordered side chains, with both polymorphs extending over at least a few nanometers. A possible overall scenario is that of a layered crystalline polymorph with crystalline side chains (phase 4) in the center and a surrounding layered crystalline polymorph with disordered side chains (phase 3), embedded in the remaining amorphous phase.

■ ASSOCIATED CONTENT

Supporting Information

Figures containing the experimental as well as theoretical temperature-dependent Stokes shift of the LEP as well as Franck−Condon analysis of aggregate absorption spectrum at 160 K, using one progression; fitted parameters E_0 and σ from the FC analysis on the coiled emission spectrum as a function of temperature; FC analysis on the site-selected emission spectra at 5 and 160 K at excitation of 2.070 and 1.865 eV as well as corresponding fraction of HEP and LEP phase. This material is available free of charge via the Internet at http://pubs.acs.org.

■ AUTHOR INFORMATION

Corresponding Author

*E-mail: anna.koehler@uni-bayreuth.de (A.K.).

Present Address

M.S.: Department of Macromolecular Chemistry, University of Freiburg, Stefan-Meier.-Str. 31, 79104 Freiburg, Germany.

Notes

The authors declare no competing financial interest.

■ ACKNOWLEDGMENTS

We acknowledge financial support by the Bavarian State Ministry of Science, Research, and the Arts through the Collaborative Research Network 'Solar Technologies go Hybrid', by the German Science Foundation DFG through the doctoral training center GRK1640 and by the Federal Ministry of Education and Research (BMBF) through the project "OLYMP". We thank Marie-Luis Panzer for the help with the TOC Graphic. Furthermore, we thank Alexander Rudnick for the assistance with the site selective measurements.

■ REFERENCES

(1) Pingel, P.; Zen, A.; Abellón, R. D.; Grozema, F. C.; Siebbeles, L. D. A.; Neher, D. *Adv. Funct. Mater.* **2010**, *20*, 2286−2295.
(2) Kline, R. J.; McGehee, M. D.; Kadnikova, E. N.; Liu, J. S.; Frechet, J. M. J. *Adv. Mater.* **2003**, *15*, 1519−1522.
(3) Paquin, F.; Latini, G.; Sakowicz, M.; Karsenti, P.-L.; Wang, L.; Beljonne, D.; Stingelin, N.; Silva, C. *Phys. Rev. Lett.* **2011**, *106*, 197401.
(4) Scharsich, C.; Lohwasser, R. H.; Sommer, M.; Asawapirom, U.; Scherf, U.; Thelakkat, M.; Neher, D.; Köhler, A. *J. Polym. Sci., Part B: Polym. Phys.* **2012**, *50*, 442−453.
(5) Koch, F. P. V.; Rivnay, J.; Foster, S.; Müller, C.; Downing, J. M.; Buchaca-Domingo, E.; Westacott, P.; Yu, L.; Yuan, M.; Baklar, M.; Fei, Z.; Luscombe, C.; McLachlan, M. A.; Heeney, M.; Rumbles, G.; Silva, C.; Salleo, A.; Nelson, J.; Smith, P.; Stingelin, N. *Prog. Polym. Sci.* **2013**, *38*, 1978−1989.
(6) Duong, D. T.; Toney, M. F.; Salleo, A. *Phys. Rev. B* **2012**, *86*, 205205.
(7) Berson, S.; De Bettignies, R.; Bailly, S.; Guillerez, S. *Adv. Funct. Mater.* **2007**, *17*, 1377−1384.
(8) Zen, A.; Saphiannikova, M.; Neher, D.; Grenzer, J.; Grigorian, S.; Pietsch, U.; Asawapirom, U.; Janietz, S.; Scherf, U.; Lieberwirth, I.; Wegner, G. *Macromolecules* **2006**, *39*, 2162−2171.
(9) Chasteen, S. V.; Carter, S. A.; Rumbles, G. *Proc. SPIE* **2005**, 59380J−59380J-11.
(10) Hiorns, R. C.; de Bettignies, R.; Leroy, J.; Bailly, S.; Firon, M.; Sentein, C.; Khoukh, A.; Preud'homme, H.; Dagron-Lartigau, C. *Adv. Funct. Mater.* **2006**, *16*, 2263−2273.
(11) Huang, Y.; Kramer, E. J.; Heeger, A. J.; Bazan, G. C. *Chem. Rev.* **2014**, *114*, 7006−7043.
(12) Kim, Y.; Cook, S.; Tuladhar, S. M.; Choulis, S. A.; Nelson, J.; Durrant, J. R.; Bradley, D. D. C.; Giles, M.; McCulloch, I.; Ha, C.-S.; Ree, M. *Nat. Mater.* **2006**, *5*, 197−203.

DOI: 10.1021/acs.macromol.5b00129
Macromolecules 2015, 48, 1543−1553

(13) Sirringhaus, H.; Brown, P. J.; Friend, R. H.; Nielsen, M. M.; Bechgaard, K.; Langeveld-Voss, B. M. W.; Spiering, A. J. H.; Janssen, R. A. J.; Meijer, E. W.; Herwig, P.; de Leeuw, D. M. *Nature* **1999**, *401*, 685−688.
(14) Brown, P. J.; Thomas, D. S.; Kohler, A.; Wilson, J. S.; Kim, J. S.; Ramsdale, C. M.; Sirringhaus, H.; Friend, R. H. *Phys. Rev. B* **2003**, *67*, 064203.
(15) Martin, T. P.; Wise, A. J.; Busby, E.; Gao, J.; Roehling, J. D.; Ford, M. J.; Larsen, D. S.; Moulé, A. J.; Grey, J. K. *J. Phys. Chem. B* **2012**, *117*, 4478−4487.
(16) Paquin, F.; Yamagata, H.; Hestand, N. J.; Sakowicz, M.; Bérubé, N.; Côté, M.; Reynolds, L. X.; Haque, S. A.; Stingelin, N.; Spano, F. C.; Silva, C. *Phys. Rev. B* **2013**, *88*, 155202.
(17) Baghgar, M.; Labastide, J. A.; Bokel, F.; Hayward, R. C.; Barnes, M. D. *J. Phys. Chem. C* **2014**, *118*, 2229−2235.
(18) Baghgar, M.; Labastide, J.; Bokel, F.; Dujovne, I.; McKenna, A.; Barnes, A. M.; Pentzer, E.; Emrick, T.; Hayward, R.; Barnes, M. D. *J. Phys. Chem. Lett.* **2012**, *3*, 1674−1679.
(19) Koch, F. P.; Heeney, M.; Smith, P. *J. Am. Chem. Soc.* **2013**, *135*, 13699−13709.
(20) Poelking, C.; Andrienko, D. *Macromolecules* **2013**, *46*, 8941−8956.
(21) Yuan, Y.; Zhang, J.; Sun, J.; Hu, J.; Zhang, T.; Duan, Y. *Macromolecules* **2011**, *44*, 9341−9350.
(22) Guo, Y.; Wang, L.; Han, Y.; Geng, Y.; Su, Z. *Polym. Chem.* **2014**, *5*, 1938−1944.
(23) Brinkmann, M. *J. Polym. Sci., Part B: Polym. Phys.* **2011**, *49*, 1218−1233.
(24) Noriega, R.; Rivnay, J.; Vandewal, K.; Koch, F. P. V.; Stingelin, N.; Smith, P.; Toney, M. F.; Salleo, A. *Nat. Mater.* **2013**, *12*, 1038−1044.
(25) Köhler, A.; Hoffmann, S. T.; Bässler, H. *J. Am. Chem. Soc.* **2012**, *134*, 11594−11601.
(26) Cone, C. W.; Cheng, R. R.; Makarov, D. E.; Vanden Bout, D. A. *J. Phys. Chem. B* **2011**, *115*, 12380−12385.
(27) Prosa, T. J.; Winokur, M. J.; McCullough, R. D. *Macromolecules* **1996**, *29*, 3654−3656.
(28) Mena-Osteritz, E.; Meyer, A.; Langeveld-Voss, B. M. W.; Janssen, R. A. J.; Meijer, E. W.; Bauerle, P. *Angew. Chem., Int. Ed.* **2000**, *39*, 2680−2684.
(29) Rahimi, K.; Botiz, I.; Stingelin, N.; Kayunkid, N.; Sommer, M.; Koch, F. P. V.; Nguyen, H.; Coulembier, O.; Dubois, P.; Brinkmann, M.; Reiter, G. *Angew. Chem., Int. Ed.* **2012**, *51*, 11131−11135.
(30) Wu, Z. Y.; Petzold, A.; Henze, T.; Thurn-Albrecht, T.; Lohwasser, R. H.; Sommer, M.; Thelakkat, M. *Macromolecules* **2010**, *43*, 4646−4653.
(31) Kline, R. J.; DeLongchamp, D. M.; Fischer, D. A.; Lin, E. K.; Richter, L. J.; Chabinyc, M. L.; Toney, M. F.; Heeney, M.; McCulloch, I. *Macromolecules* **2007**, *40*, 7960−7965.
(32) Köse, M. E. *J. Phys. Chem. C* **2011**, *115*, 13076−13082.
(33) Lohwasser, R. H.; Thelakkat, M. *Macromolecules* **2011**, *44*, 3388−3397.
(34) Kohn, P.; Huettner, S.; Komber, H.; Senkovskyy, V.; Tkachov, R.; Kiriy, A.; Friend, R. H.; Steiner, U.; Huck, W. T. S.; Sommer, J.-U.; Sommer, M. *J. Am. Chem. Soc.* **2012**, *134*, 4790−4805.
(35) Panzer, F.; Bässler, H.; Lohwasser, R.; Thelakkat, M.; Köhler, A. *J. Phys. Chem. Lett.* **2014**, *5*, 2742−2747.
(36) Lebedev, B. V.; Rabinovich, I. B.; Milov, V. I.; Lityagov, V. Y. *J. Chem. Thermodyn.* **1978**, *10*, 321−329.
(37) Hotta, S.; Rughooputh, S. D. D. V.; Heeger, A. J.; Wudl, F. *Macromolecules* **1987**, *20*, 212−215.
(38) Ho, P. K. H.; Kim, J.-S.; Tessler, N.; Friend, R. H. *J. Chem. Phys.* **2001**, *115*, 2709−2720.
(39) Clark, J.; Silva, C.; Friend, R. H.; Spano, F. C. *Phys. Rev. Lett.* **2007**, *98*, 206406.
(40) Spano, F. C. *J. Chem. Phys.* **2005**, *122*, 234701.
(41) Spano, F. C. *Chem. Phys.* **2006**, *325*, 22−35.
(42) Spano, F. C. *Acc. Chem. Res.* **2010**, *43*, 429−439.
(43) Spano, F. C.; Clark, J.; Silva, C.; Friend, R. H. *J. Chem. Phys.* **2009**, *130*, 074904.
(44) Clark, J.; Chang, J. F.; Spano, F. C.; Friend, R. H.; Silva, C. *Appl. Phys. Lett.* **2009**, *94*, 163306.
(45) Yamagata, H.; Spano, F. C. *J. Chem. Phys.* **2012**, *136*, 184901.
(46) Yamagata, H.; Hestand, N. J.; Spano, F. C.; Köhler, A.; Scharsich, C.; Hoffmann, S. T.; Bässler, H. *J. Chem. Phys.* **2013**, *139*, 114903.
(47) Martín, J.; Nogales, A.; Martín-González, M. *Macromolecules* **2013**, *46*, 1477−1483.
(48) Brambilla, L.; Tommasini, M.; Botiz, I.; Rahimi, K.; Agumba, J. O.; Stingelin, N.; Zerbi, G. *Macromolecules* **2014**, *47*, 6730−6739.
(49) Hugger, S.; Thomann, R.; Heinzel, T.; Thurn-Albrecht, T. *Colloid Polym. Sci.* **2004**, *282*, 932−938.
(50) Bässler, H. *Phys. Status Solidi B* **1993**, *175*, 15−56.
(51) Hoffmann, S. T.; Bässler, H.; Koenen, J.-M.; Forster, M.; Scherf, U.; Scheler, E.; Strohriegl, P.; Köhler, A. *Phys. Rev. B* **2010**, *81*, 115103.
(52) Bjorgaard, J. A.; Kose, M. E. *J. Phys. Chem. C* **2014**, *118*, 5756−5761.
(53) Athanasopoulos, S.; Emelianova, E. V.; Walker, A. B.; Beljonne, D. *Phys. Rev. B* **2009**, *80*, 195209.

DOI: 10.1021/acs.macromol.5b00129
Macromolecules 2015, 48, 1543−1553